NANO · MICRO small
www.small-journal.com

In Vivo Kidney Allograft Endothelial Specific Scavengers for On-Site Inflammation Reduction under Antibody-Mediated Rejection

Chang Liu, Pengpeng Yan, Xiaoyu Xu, Wenhui Zhou, Dhayakumar Rajan Prakash, Shuqi Wang, Junnian Zhou, Rending Wang, Hongfeng Huang, Jianghua Chen, Hongbo Zhang, and Jia Shen**

Kidney transplantation is the most effective therapy for patients with end-stage renal disease. However, antibody-mediated rejection (ABMR) threatens long-term survival of renal grafts. Although ABMR can be controlled by donor-specific antibody clearance and B- or (and) plasma-cells inhibition, the treatment often causes severe side effects in patients. Therefore, there is need to explore site-specific scavengers. In this study, a nanovehicle carrying an anti-inflammatory drug is developed with complement component 4d targeting, a specific biomarker expressed on allograft endothelium under ABMR. Moreover, the nanovehicle is endowed with photothermal properties to control drug release. Analysis through systematic in vitro and in vivo toxicity, non-invasive targeted imaging, and in situ remote controlled drug release show the nanovehicle specifically targets allograft kidney endothelium, releases an anti-inflammatory drug, methylprednisolone, locally upon laser irradiation, and promotes recovery of injured endothelium, without affecting systemic inflammation or innate immune responses. This strategy has the potential for future clinical application in ABMR treatment.

1. Introduction

End-stage renal disease is a global public health concern. Studies report increase in incidence of end-stage renal disease due to the progressive growth of the world's population with chronic kidney disease and high-risk factors such as global aging, increasing prevalence of diabetes and obesity.[1] Kidney transplantation (KT) is most effective mode of treatment for end-stage renal disease compared with hemodialysis and peritoneal dialysis. Novel immunosuppressive agents have been developed to improve one-year transplant survival rate, however, they have limited long-term outcomes. Allograft rejection, including acute/chronic antibody-mediated rejection (ABMR) and acute/chronic cell-mediated rejection, significantly affect success of KT

C. Liu, P. Yan, R. Wang, H. Huang, J. Chen, J. Shen
Kidney Disease Center
The First Affiliated Hospital
College of Medicine
Zhejiang University
Hangzhou 310003, China
E-mail: jiashen@zju.edu.cn

C. Liu, X. Xu, W. Zhou, D. R. Prakash, H. Zhang
Pharmaceutical Sciences Laboratory
Åbo Akademi University
Turku 20520, Finland
E-mail: hongbo.zhang@abo.fi

C. Liu, X. Xu, W. Zhou, H. Zhang
Turku Bioscience Centre
University of Turku and Åbo Akademi University
Turku 20520, Finland

The ORCID identification number(s) for the author(s) of this article can be found under https://doi.org/10.1002/smll.202106746.

DOI: 10.1002/smll.202106746

X. Xu
ENT institute and Department of Otorhinolaryngology
Eye & ENT Hospital
State Key Laboratory of Medical Neurobiology
Institutes of Biomedical Sciences
Fudan University
Shanghai 200031, China

S. Wang
Institute for Translational Medicine
Zhejiang University
Hangzhou, Zhejiang Province 310029, China

J. Zhou
Experimental Hematology and Biochemistry Lab
Beijing Institute of Radiation Medicine
Beijing 100850, China

J. Zhou
Stem Cell and Regenerative Medicine Lab
Institute of Health Service and Transfusion Medicine
Beijing 100850, China

H. Zhang
Department of Orthopaedics
Shanghai Key Laboratory for Prevention and Treatment of Bone and Joint Diseases
Shanghai Institute of Traumatology and Orthopaedics
Ruijin Hospital
Shanghai Jiao Tong University School of Medicine
Shanghai 200025, China

therapy. ABMR presents a high incidence and leads to graft loss and regression of renal dialysis treatment.[2] Chronic ABMR is currently the most common cause of post-transplant renal failure.[3] Moreover, administration of high-dose inflammation suppressive agents against ABMR, such as corticosteroid, results in several systemic side effects, including peptic ulcer, infection and steroid diabetes.[4] If targeted inflammation suppression is administered at the site of allograft kidney, it may greatly improve the treatment outcome and reduce side-effects under allograft rejection.

In nowadays clinical practice, the complement component 4d (C4d) is regarded as one of the most important pathological diagnostic biomarker for ABMR.[5] C4d is presented at a higher level on activated endothelium in human leukocyte antigens-derived ABMR compared with other complement components, even it has no biological function itself.[6] C4d is proved co-localizing with the membrane attack complexes (MACs) which enhance the P-selectin secretion and recruit inflammatory cell infiltration.[7] Therefore, C4d is a good candidate target for anti-inflammatory drug delivery in AMBR.[8]

Nanotechnology-based drug delivery and therapy has revolutionized traditional therapy approaches, and can be used to control delivery of various drugs to specific sites spatiotemporally. Various nanocarriers, such as lipid-based assemblies,[9] DNA nanostructures,[10] polymeric nanogels[11] and inorganic nanoparticles[12] can significantly improve effectiveness and selectivity of drug delivery in vivo. Moreover, nanocarriers can be used for controlled drug release under heat,[13] light,[14] pH,[15] and other responses. In addition, nanoparticles can be utilized as imaging agents to support in vivo labelling and diagnostics.[16] Silica has been labelled as "generally recognized as safe" by the US Food and Drug Administration due to its excellent biocompatibility, making it highly prospective for further use in clinical application. Mesoporous silica nanoparticle (MSN) is an ideal material for loading guest molecules of various sizes, shapes and functions owing to their unique structural characteristics such as tunable pore size, high accessible pore volume and well-defined surface functionalization.[17] MSN-based smart nanocarriers have been explored through a variety of "stimulus responses" and "gatekeepers" construction strategies, which allow them to modulate release of cargo at a desired location and for a specific period of time. To achieve this effective and controlled release, it is necessary to select the appropriate stimulus response mode. Notably, near-infrared (NIR) light-induced photothermal response systems have been widely used as a mild but efficient stimulus response strategy for on-demand drug delivery, owing to the non-invasive approach, high spatial resolution for in vivo treatment and minimal damage to normal tissues.[18] Transition metal semiconductor nanocrystals with high NIR absorption, such as copper sulfide (CuS) nanoparticles, are promising photothermal agents, mainly due to their localized surface plasmon resonance generated by d–d energy band transition.[19] CuS nanoparticles are also biodegradable and have a lower long-term toxicity compared with most commonly used gold nanorods, thus they provide a clinically favorable material for photothermal applications.[20] Thermosensitive polymers used as "gatekeepers", mainly the newly disclosed poly(N-isopropylacrylamide-co-methacrylic acid) (PNIPAm/MAA, PNcM), are thermosensitive by the coil-to-globule transition of the polymer chains in physiological solution, which undergoes a low critical solution temperature. The stretched and hydrophilic polymer chains in solution tend to contract into a very compact cluster at above low critical solution temperature. The phase transition temperature of PNcM is higher compared with the body temperature which is conducive for drug delivery but it is low enough, at 45°C to prevent damage of tissue components[21] thus it has high potential for further clinical application.[22] Therefore, the ultimate aim of constructing CuS/MSN/PNcM core–shell materials with photothermal responsiveness is to control the opening and closing of the pores through intermittent heating and thus the release of the loaded molecules.

In the current study, a nanocarrier was developed for in vivo injured renal vascular endothelial targeting to treat ABMR at the allograft site after kidney transplantation. Water-soluble CuS nanoparticles were used as the core of the nanosystem to enable the NIR response (**Figure 1**).[23] Mesoporous silica nanoshells with controllable thickness and pore size were introduced on the surface of CuS to serve as drug reservoir. The thermosensitive polymer poly(N-isopropylacrylamide-co-methacrylic acid, PNcM) was coated on the drug-loaded CuS@MSN (CuS@MSN@PNcM, referred as NP) by electrostatic nanoprecipitation to avoid leakage and to remotely control drug release. The NP was then surface functionalized by C4d antibody (C4dAb) to form the final nanocomposite NP-C4dAb. The drug loading efficiency, drug release profile with and without NIR irradiation, in vitro cytotoxicity, in vitro and in vivo vascular endothelial targeting, NIR triggered photothermal responsive drug release and therapeutic effects, in vivo long-term toxicity and the reducing of systemic site effects were then explored.

2. Results and Discussion

2.1. Preparation and Characterization of Nanoparticles

Copper sulfide nanoparticles (CuS) are new type of photothermal agents with good photothermal conversion capabilities due to their properties as p-type semiconductors.[24] Mesoporous silica nanoparticles (MSN) display controllable porosity size, high surface area and large volume of pores, and are amenable to superficial modification.[25] Therefore, MSN has been investigated as drug vector since 2001.[26] The synthetic positively charged CuS coated with cetyltrimethylammonium chloride (CTAC) (as CuS-CTAC) was used to encapsulate the MSN shell on CuS particles . Transmission electron microscopy (TEM, **Figure 2**A) image of CuS-CTAC show an average particle size of about 12 nm. Dynamic light scattering (DLS) and zeta potential measurements reveal an average particle dimension of 24.36 ± 5.47 nm and a surface charge of 19.3 ± 0.5 mV (Figure S1A, Supporting Information). The surfactant CTAC was utilized here not only as a capping agent to stabilize the CuS, but also as a soft template to induce the growth of MSN shell on CuS successfully. The core–shell structure of CuS@MSN (Figure 2B) has a particle size of 90 nm. The size of CuS@MSN increased to 105.70 ± 9.94 nm as shown by DLS measurement, and the surface charge of CuS@MSN changed significantly, from positive to negative (-11.3 ± 0.5 mV) as determined by zeta

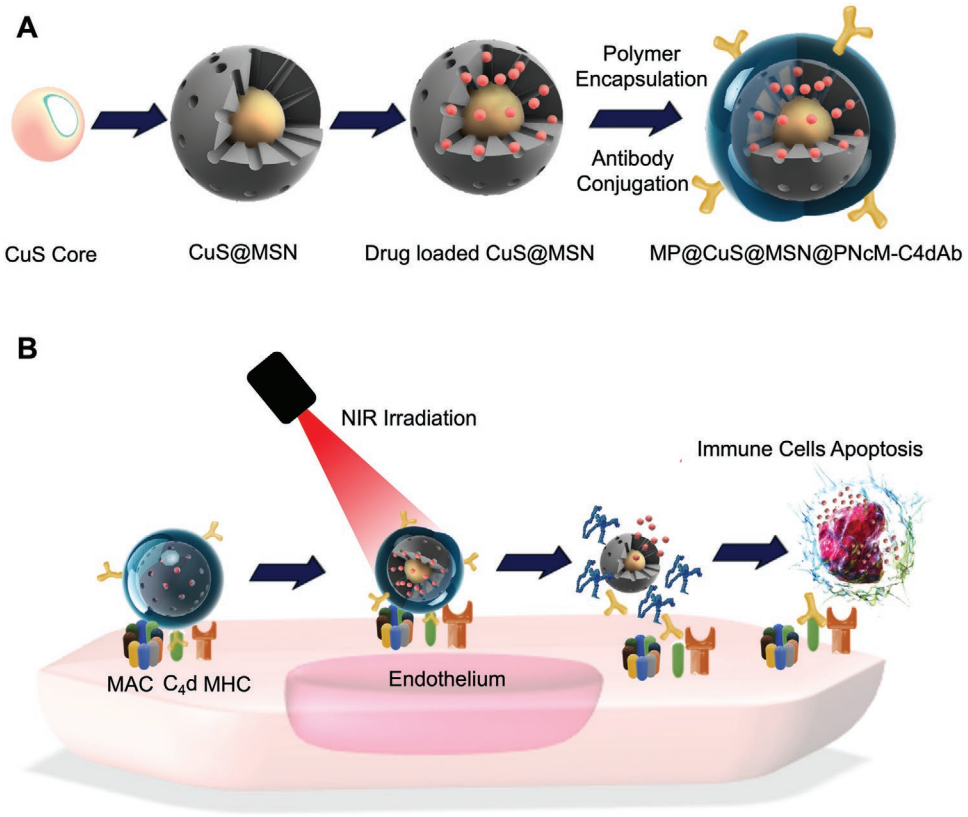

Figure 1. The study design, synthetic route and working principle. A) The scheme describing synthesis of MP@CuS@MSN@PNcM-C4dAb (MP-NP-C4dAb, NP stands for CuS@MSN@PNcM). B) C4d targeted nanoparticles with NIR responsive drug release to deliver methylprednisolone to local allograft endothelium cells and induce immune cell apoptosis.

potential compared with CuS-CTAC (Figure S1B, Supporting Information). The surfactant CTAC was extracted by soaking the nanoparticles in methanol with 1.0 wt% NaCl at ambient temperature. Fourier transform infrared (FTIR) spectroscopy analysis demonstrate complete removal of the surfactant CTAC as the characteristic C-H peak in the wavelength range of 2800 cm^{-1} was not present in the surfactant-extracted CuS@MSN sample (Figure S2, Supporting Information).[27] Modification of amino groups was performed on the CuS@MSN lacking the template by reacting with (3-aminopropyl)triethoxysilane (APTEOS) for 48 h at room temperature to attach functional polymers to the surface of CuS@MSN for in vivo drug delivery and controlled drug release. Presence of a 3000 cm^{-1} N-H peak of APTEOS showed successful surface modification (Figure S2, Supporting Information). Size and morphology of the modified CuS@MSN showed no significant differences compared with the CuS@MSN before surface modification, however, the surface charge changed to positive (11.5 ± 0.6 mV).

The photothermal properties of the synthesized nanoparticles were assessed under the radiation of near infrared light (NIR). In this study, 808 nm light source was employed to explore the photothermal conversion of CuS-based nanoparticles because of their high absorption at 808 nm, in addition to their deeper penetration into tissues and better conservation limits for human skin. The synthesized CuS@MSN was verified further by its characteristic green color and strong absorption around 808 nm in the UV-Vis absorption spectrum (Figure 2D). Furthermore, the photothermal images show an effective energy conversion from NIR to heat via the nanoparticles (Figure 2D, insert), while the control (water) shows merely a slight temperature increase after the equivalent time of laser irradiation. The quantitative temperature variation of CuS@MSN in aqueous solution was explored in relation to the laser exposure time. The temperature variation of CuS@MSN at different concentrations (0, 0.5, 1.0, 2.0, and 4.0×10^{-3} M) irradiated with 808 nm NIR laser (2.0 W cm^{-2}) for 900 s is presented in Figure 2E. The temperature change was negligible in pure water regardless of the irradiation time. However, for the sample containing CuS@MSN, the temperature increases significantly with increase in particle concentration and increase in irradiation time, mainly within the first 6 min. Notably, further increase in irradiation time showed gradual increase in temperature and condensed water vapor were observed on the well wall (Figure 2F). The findings for 4.0×10^{-3} M CuS@MSN showed a temperature increase from 22.4 to a steady-state of 65.3°C during the ramp-up, demonstrating the rapid and efficient energy conversion from NIR laser to heat. To explore the effect of laser power density on temperature rise, the CuS@MSN samples with fixed concentration (4.0×10^{-3} M) were exposed to the laser at different power densities (0.5, 1.0, 1.5, and 2.0 W cm^{-2}) for 15 min. The ramp-up curves displayed a clear laser power-dependent photothermal characteristic of

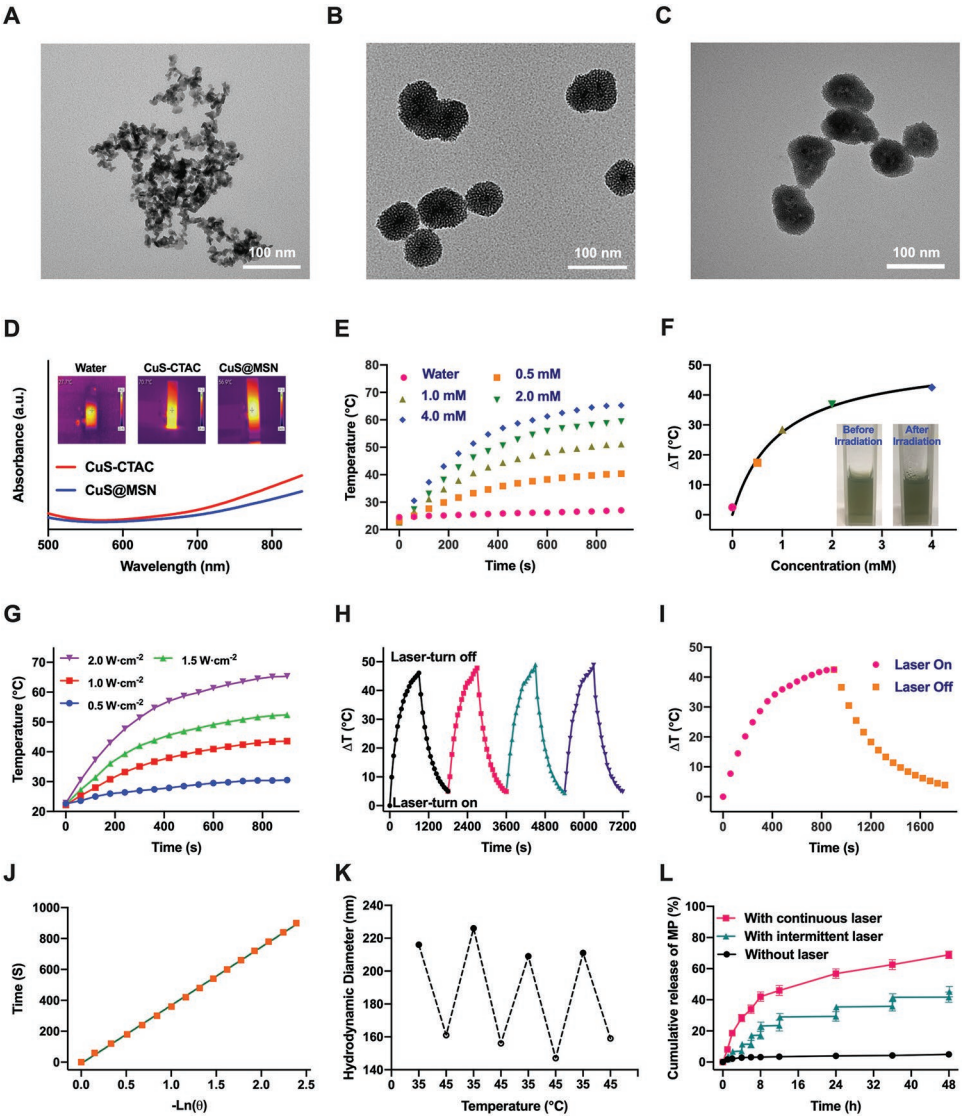

Figure 2. The physicochemical characterization and drug release profiles of nanoparticles. A–C) The TEM images of CuS-CTAC, CuS@MSN and CuS@MSN@PNcM. D) UV-vis absorption and photothermal images of CuS-CTAC and CuS@MSN. E) Temperature variation of CuS@MSN solution versus 808 nm laser irradiation time. F) Temperature difference (Δ*T*) versus the concentration of CuS@MSN solution over 900 s. G) Temperature changes of CuS@MSN nanoparticles with a fixed concentration (4.0×10^{-3} M) versus laser power densities. H) Temperature rise of CuS@MSN solution during four laser switching cycles. I) The photothermal response of the CuS@MSN solution with and without laser over 900s. J) Heat dissipation time constants calculated by plotting the negative natural logarithm (-lnθ) of the cooling period with time. K) The mean hydrodynamic diameters of NP versus temperature by DLS. L) Methylprednisolone (MP) release profile of MP-NP under various laser irradiation conditions (intermittent irradiation 300 s).

CuS@MSN, with increase in temperature to 52.4 and 65.3°C at 1.5 and 2.0 W cm^{-2}, respectively (Figure 2G). Based on these findings, 2.0 W cm^{-2} was chosen for further experiments. Besides the photothermal converting ability, the photothermal stability of the materials is also important in this drug delivery system. The temperature changes during the heating/cooling process were recorded for four consecutive cycles (Figure 2H). The findings showed that increase in temperature was effectively maintained over the four cycles tested, indicating that CuS@MSN has a highly stable photothermal conversion capability. The excellent photothermal conversion capability and stability performance indicate that CuS@MSN is an outstanding candidate material for future biological uses. Further, the photothermal conversion efficiency (η) of CuS@MSN was determined. The η values were calculated (see Supporting Information experimental procedures for details) as follows:[28]

$$\eta = \frac{hA\Delta T_{max} - Q_s}{I\left(1-10^{-A_\lambda}\right)} \quad (1)$$

where h indicates the heat transfer coefficient, A represents the surface area of the vessel, ΔT_{max} represents the temperature variation of the CuS@MSN nanoparticles solution at the maximum steady-state temperature, I represents the laser power, A_λ represents the absorbance of CuS nanoparticles

at 808 nm, Q_s indicates the heat associated with the light absorbance of the solvent, and η represents the photothermal conversion efficiency. According to Equation (1) (Figure 2I,J), the 808 nm laser η of CuS@MSN was determined to be 41.9%, implying that it can be used as an effective photothermal conversion agent.

Further analysis showed that the synthesized CuS@MSN under the coating of MSN maintained the photothermal conversion property and served as a drug delivery system for anti-inflammation. The small molecule drug methylprednisolone (MP) was loaded as an anti-inflammatory agent into CuS@MSN in methanol solution under stirring. A standard curve for the drug was generated (Figure S3, Supporting Information), the findings showed that after 24 h of infiltration, the loading of MP reached 326.1 mg g^{-1}. Poly(N-isopropylacrylamide-co-methacrylic acid), a commonly used thermoresponsive polymer with a relatively low critical solution temperature of ≈45°C in water[29] was used to induce temperature sensitive property to CuS@MSN and also to minimize leakage of drug from the nanocomposite. After loading the drug, CuS@MSN was then transferred to PNcM aqueous solution for encapsulation since MP is insoluble in water. PNcM layer was observed to be deposited on CuS@MSN (Figure 2C) due to the different electron penetration of the core inorganic CuS@MSN and the polymer on the surface. FTIR spectroscopy analysis showed successful coating of CuS@MSN, as evidenced by presence of PNcM peak in NP (Figure S2, Supporting Information). The mean hydrodynamic size of the nanoparticles was determined by DLS as a function of temperature. The diameter of the nanoparticles decreases when heated to 45°C and recovers to their initial value when cooled to 35°C (Figure 2K), which is a reproducible thermal-responsive size change. The temperature-induced size change (expansion and contraction of the thermosensitive polymer absorbed at the surface) indicated that this material has the ability to control drug release, taking advantage of the NP under intermittent 808 nm laser irradiation. Figure 2L shows the in vitro release profile of the NP loaded with MP (MP-NP) in PBS buffer against temperature variations from 35 to 45°C. Without irradiation, only 4.0% of the contained drug was released after 24 h, with no significant change over several hours due to the confinement of the loose polymer brush, except for a small burst release initially caused by the drug on the surface. The rapid release of MP with continuous NIR irradiation was compatible with the hydrophobic contraction of PNcM brushes. At physiological pH and 45°C, the platform exhibited an efficient release capability with a 68.9% cumulative release in 48 h. The photothermal effect of CuS@MSN that is the instantaneous rise in temperature under laser irradiation 300 s, accelerated release of MP from NP at 35°C. Release of MP was controlled by intermitted irradiation, which provides a mechanism to control drug release flux to achieve the desired biological effect.

2.2. In Vitro Toxicity, Targeting and Therapeutic Assay

Cytotoxicity of drug loaded NP with/without laser (MP-NP and MP-NP + Laser) was determined for cytocompatibility of the drug delivery system. The findings showed that viability of mouse primary kidney glomerular endothelial cells (mGEnCs) was at 70% even after treatment with free MP at a high concentration of 200 μg mL^{-1} (Figure S4, Supporting Information). In addition, MP-NP carrier exhibited similar toxicity to mGEnCs after 12 h of incubation without irradiation, indicating that NP was safe and biocompatible for drug delivery. The cytotoxic effect of MP-NP under NIR irradiation was slightly increased with increase in drug concentration compared with that of MP-NP in the absence of irradiation, which can be attributed to increase in concentration of drug released suddenly from the NP by NIR irradiation. The findings showed similar cell mortality rates for MP-NP + Laser group compared with that in MP group for 0 to 175 μg mL^{-1} concentration range, indicating that the heat generated by photothermal conversion did not cause further injury to the endothelial monolayer which aggravates inflammation in graft.

Donor specific anti-major histocompatibility complex antibodies (DSA) attacks the capillary endothelium surface through complement fixation and MACs assembly.[30] The surface inserted MACs promote multiple endothelium activation signals and arachidonic acid metabolism cascades to trigger inflammation response and lymphocytes infiltration through the endothelium cell layer in situ.[31] Therefore, it is important to explore the potential or activated attack site at the early stage of this process in ABMR for reduction of inflammation and graft injury. In clinical practice, the complement component 4d (C4d) is an important prognostic biomarker in ABMR and studies report that it colocalizes with mismatched human leukocyte antigens, where high exposure human leukocyte antigens density and MACs are present.[32] Approximately 33% of acute rejection grafts and over 60% chronic ABMR attacked grafts are C4d positive. Furthermore, the C4d positive rate can reach 100% in cases of transplanted renal thrombotic microangiopathy and transplant-related glomerular lesions.[33] In the current study, C4d was targeted for MP-NP nanocomposites in vitro and in vivo. Identification of inflamed cell is a key prerequisite for in vivo vascular endothelial targeting and for improving drug treatment efficacy. Complement activated mGEnCs were used for targeting study of C4dAb-conjugated NPs. The red fluorescent dye Sulfo-Cyanine 5.5 NHS ester (Cy5.5) was mixed with the precursor of nanoparticles, during synthesis of CuS@MSN, which was encapsulated in the nucleus of NP (Cy5.5-NP) to track the cellular targeting process. C4d antibody (C4dAb) was then conjugated to Cy5.5-NP (Cy5.5-NP-C4dAb) via a reaction between the carboxyl groups of PNcM on NP and the amino groups of C4dAb. The bonding efficiency of C4dAb was quantified by polyacrylamide gel electrophoresis through comparison with the bovine serum albumin standards (Figure S5, Supporting Information). The findings showed that only a small amount of free antibody was present in the PBS supernatant, most of which was coupled on the NP surface. The in vitro targeting capability of the antibody-modified nanoparticles was assessed by immunofluorescence (IF), where the artificial colors of green, red, and blue in the IF images were assigned to the fluorescent signals obtained by a confocal microscopy in the FITC (FITC-C4dAb), Cy5.5 (Cy5.5-NP-C4dAb), and Hoechst (cell nuclear) channels, respectively (**Figure 3**A). FITC signal was observed in mGEnCs after complement activation and was absent in the blank group, indicating that some cells became C4d positive after stimulation

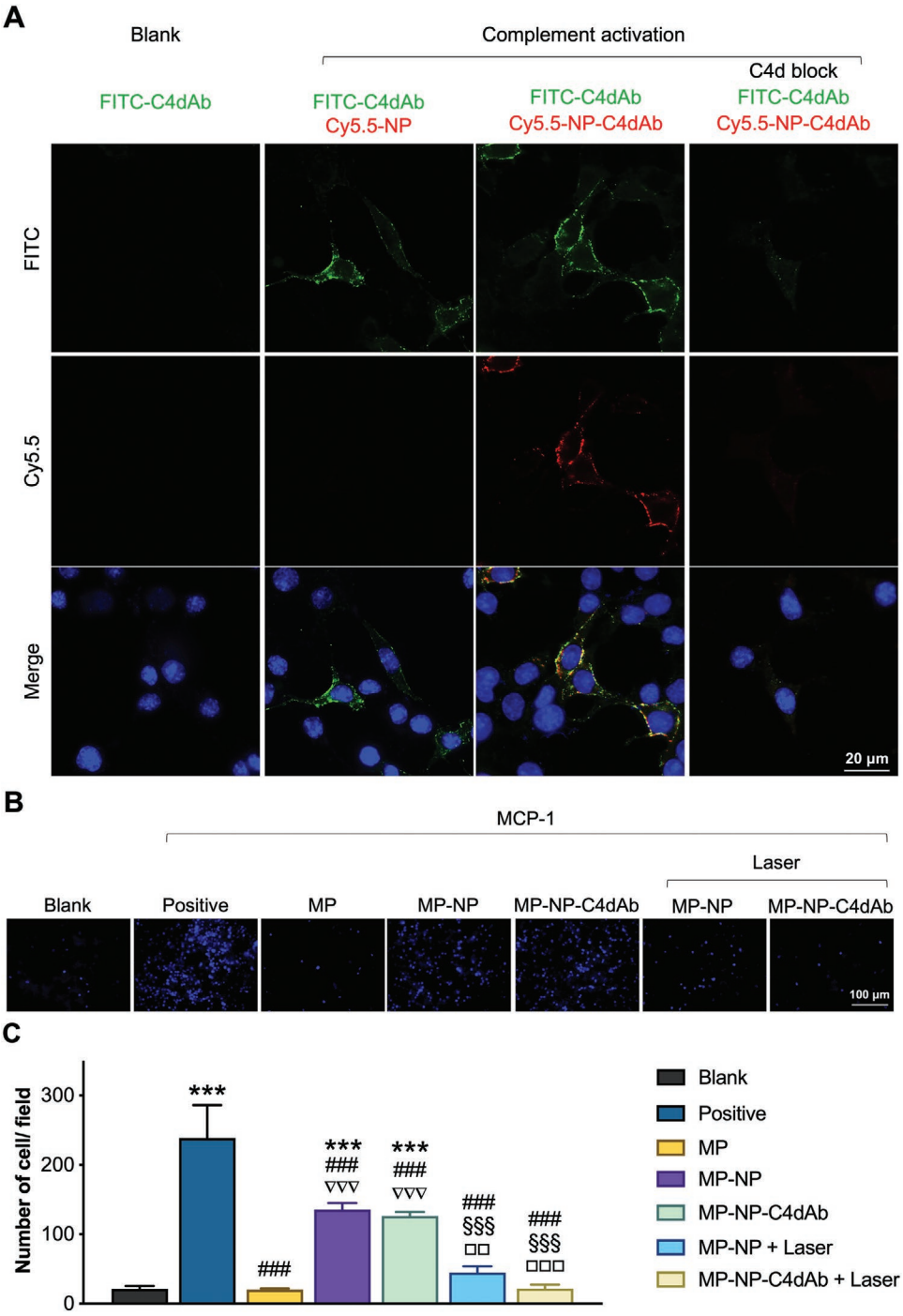

Figure 3. In vitro targeting and treatment efficacy assessment. A) Representative confocal images of mGEnCs following immunofluorescence staining and nanoparticle targeting, the green, red, and blue fluorescence indicate C4d positive, Cy5.5-NP-C4dAb nanoparticle, and cell nuclear. B) Transwell migration assay of lymphocytes across mGEnCs monolayer. C) A statistical graph of migrating lymphocytes on mGEnCs monolayer ($n = 3$, $^{***}P < 0.001$ versus Blank. $^{\#\#\#}P < 0.001$ versus Positive. $^{\triangledown\triangledown\triangledown}P < 0.001$ versus MP. $^{\S\S\S}P < 0.001$ versus MP-NP. $^{\square\square}P < 0.01$, $^{\square\square\square}P < 0.001$ versus MP-NP-C4dAb, One-way ANOVA with Tukey's multiple comparisons test).

with complement enriched serum. An intense red signal was observed in C4d positive cells after co-incubation with Cy5.5-NP-C4dAb indicated by colocalization of the red (Cy5.5) and green (FITC-C4dAb) fluorescence. However, Cy5.5 signal was not observed in the cells with co-incubation with Cy5.5-NP indicating that the cell binding of Cy5.5-NP was specific for C4dAb. In addition, the FITC-C4dAb and Cy5.5-NP-C4dAb were not observed after blocking the C4d with antibody.

After endothelial activation, MACs enhanced secretion of IL-8 and MCP-1 which induces lymphocytes migration resulting

in local inflammation. To mimic this pathological process, the invasion of lymphocytes through endothelial monolayer induced by MCP-1 was assessed in vitro using Transwell assay (Figure S6, Supporting Information). The positive group (MCP-1 +, Figure 3B, C) showed higher number of infiltrating lymphocytes compared with the blank group (MCP-1 -, Figure 3B,C), indicating the effective chemotactic capability of MCP-1 for lymphocytes. Then the anti-MCP-1-induced invasion effect of methylprednisolone and drug-loaded nanoparticles were explored. A significant reduction of migrating cells after drug administration was observed compared with the positive group, indicating a high anti-invasion effect of MP on lymphocytes. Nanoparticles (MP-NP and MP-NP-C4dAb) loaded with equal amounts of drug were added but did not show immunosuppressive effects due to the negligible drug release. On the contrary, the MP loaded NPs significantly inhibited infiltration of lymphocytes after NIR irradiation, indicating precise laser-controlled drug release. Notably, the findings did not show significant difference between NP with and without C4d because of the limited culture and reaction volume in the Transwell chamber.

2.3. In Vivo Vascular Endothelium Targeting

In vivo imaging is a method for non-invasive visualization of living organisms for research or diagnostic purposes. Labeling nanoparticles with fluorescent probes are an effective method for noninvasive assessment of their pharmacokinetics and biodistribution. Pre-sensitized C57BL/6 mice were employed as BALB/c strain derived kidney recipient to produce ABMR-attacking allograft. C4d signal was observed on the endothelium lumen side after 3 days of transplantation. In vivo activated endothelium targeted imaging was performed on C57BL/6 recipient mice after allogeneic kidney transplantation from BALB/c (Allo-KT) or C57BL/6 (Iso-KT) donor mice.[34] Mice were intravenously administered with Cy5.5-NP-C4dAb or Cy5.5-NP (5 mg/kg/200 µL) through the tail vein. Images were then obtained at 4 h post injection to explore the C4d targeting efficacy and biodistribution patterns (**Figure 4**A and Figure S7: Supporting Information). Analysis of Cy5.5 signals showed that Cy5.5-NP-C4dAb mainly accumulated in the BALB/c kidney grafts (allografts), and only a few were observed in the C57BL/6 (isograft), but none was present in the native kidneys, while no accumulation of Cy5.5-NP was observed in both allograft/isograft and native kidneys. Immunofluorescence studies of the graft kidneys were performed, and the results were consistent with IVIS results. Weak C4d positive (C4d-FITC) signals were obtained in isografts in some peritubular capillaries (PTC), indicating that ischemia/reperfusion injury had occurred during transplantation operation which induced mild to moderate endothelium injury and complement activation. Moreover, significantly higher C4d positive signals produced by complement activation were obtained on the vascular endothelium lumen side in the allograft kidneys. Notably, Cy5.5-NP-C4dAb and C4d-FITC signals were colocalized with

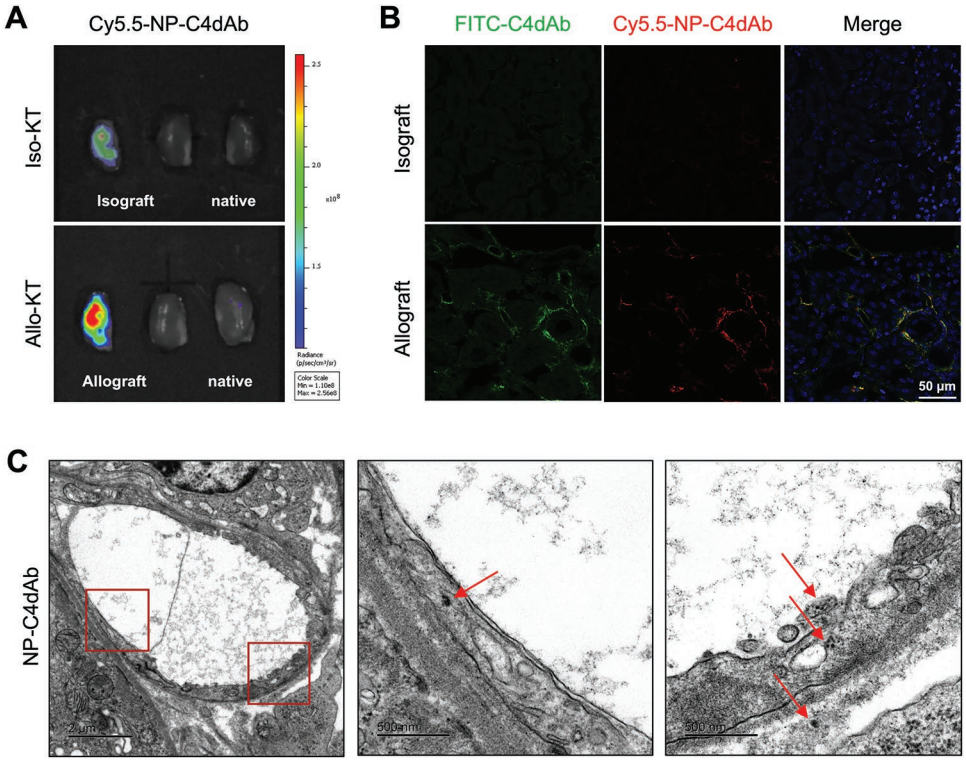

Figure 4. In vivo targeted imaging and biodistribution of nanoparticles. A) In vivo imaging of nanoparticles distribution in Isograft, Allograft and native kidney. B) Representative confocal images of sectioned Isograft and Allograft following nanoparticle targeting and immunofluorescence staining. C) TEM images of NP-C4dAb nanoparticles (red arrows) in the renal vascular endothelium.

each other (Figure 4B). Furthermore, allografts were cryosectioned and imaged under TEM. NP-C4dAb nanoparticles were observed inside the endothelium vesicles in a vascular lumen region, indicating that the C4dAb-coated nanoparticles entered the endothelial cells through a targeting-mediated process (Figure 4C). These findings indicate successful in vivo specific vasculature targeting of NP-C4dAb.

2.4. In Vivo Therapeutic Effects of Nanoparticles and Systemic Lymphopenia

Further analyses were conducted to explore in vivo drug release and therapeutic effects under NIR irradiation. The premise for effective drug release and treatment is based on the high targeting ability of the photothermal nanoparticles to the injury region, which maintained a high concentration of nanoparticles at the targeted site but not on other intact tissues. The inner aggregated thermal effect produced by photosensitive agent leads to a transitory increase in temperature at the targeted area, which initiates the phase transition of the thermosensitive polymer and results in release of the drug. Blood flow in the intravascular lumen played a cooling role during the phase transition, and no thermal damage was detected in the target tissue for the NIR treated grafts. Therapeutic effect of MP loaded nanoparticles as inflammation suppressor in vivo was explore by histopathological, immunohistochemical, and flow cytometry analysis owing to good photothermal conversion, C4d targeting, and stimuli-responsive drug release (**Figure 5**A,B). Periodic acid-Schiff (PAS) stained paraffin sections and anti-CD45 stained frozen sections showed that infiltrated lymphocytes burst out in glomeruli, capillaries, and interstitium for

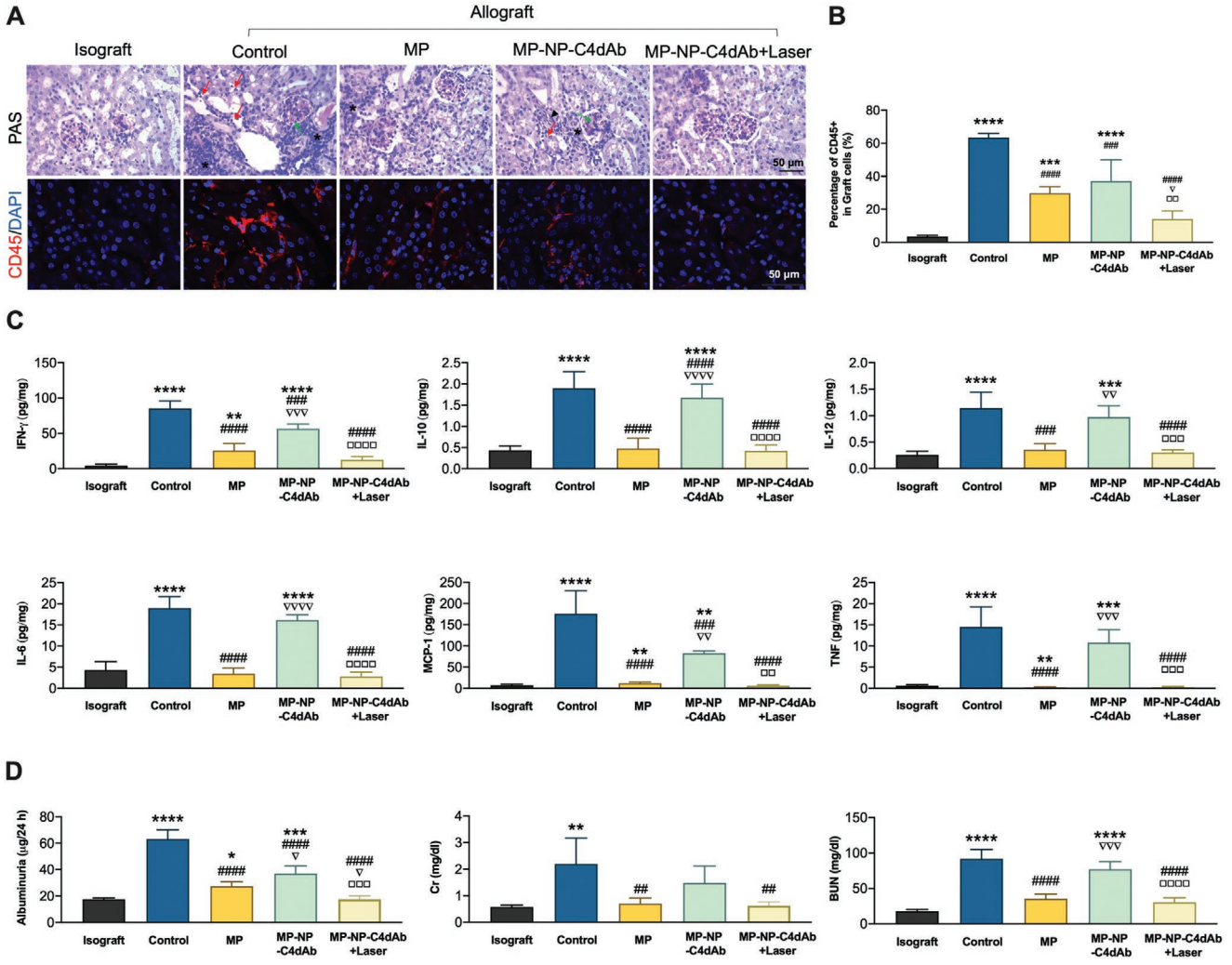

Figure 5. In vivo immunosuppression and evaluation of allograft function. A) PAS staining of paraffin tissue and CD45 immunostaining of frozen tissue showing the extent of inflammatory infiltration. In the PAS staining, the red arrow indicated peritubular capillaritis (PTC), the green arrow indicated glomerulitis, the arrowhead indicated intimal arteritis, and the asterisk indicated inflammatory cell infiltration. B) Quantitative analysis of CD45+ cells by flow cytometry. C,D) Levels of pro-inflammation factors in the graft and albuminuria in urine, creatinine (Cr) and blood urea nitrogen (BUN) levels in the graft blood were all measured ($n = 4$, $^{*}P < 0.05$, $^{**}P < 0.01$, $^{***}P < 0.001$, $^{****}P < 0.0001$ versus Isograft. $^{\#\#}P < 0.01$, $^{\#\#\#}P < 0.001$, $^{\#\#\#\#}P < 0.0001$ versus Control. $^{\triangledown}P < 0.05$, $^{\triangledown\triangledown}P < 0.01$, $^{\triangledown\triangledown\triangledown}P < 0.001$, $^{\triangledown\triangledown\triangledown\triangledown}P < 0.0001$ versus MP. $^{\square\square}P < 0.01$, $^{\square\square\square}P < 0.001$, $^{\square\square\square\square}P < 0.0001$ versus MP-NP-C4dAb, One-way ANOVA with Turkey's multiple comparisons test.)

the allograft without treatment. In addition, protein casts were detected and the amount of CD45 positive (CD45+) lymphocyte population was more than half of total graft cells as shown by flow cytometry. Notably, drug administration significantly decreased the number of infiltrated lymphocytes, and the pathological analysis showed mild and diffused interstitium inflammation in the MP treated group. MP-NP-C4dAb without laser irradiation showed less anti-inflammatory effect compared with equivalent dose of MP alone. Moreover, focal sever and diffused interstitium inflammation and glomerulitis were detected in the sections. Level of CD45+ lymphocyte in MP group was lower compared with that of the untreated allografts, but the level was higher compared with that observed in isografts. Use of laser irradiation to activate the drug release from MP-NP-C4dAb at the allograft site showed a significant decrease in the CD45+ population to the same level as that of isografts. Similar findings were observed in the PAS staining experiments, and only few inflammatory events were observed in the allograft sections in the laser treated MP-NP-C4dAb group. The findings showed no endothelial cell swelling or apoptosis and tissue edema or inflammation, indicating that the laser was sufficiently mild to induce drug release without causing damage to the transplanted kidney tissue. In addition, the effect of MP and MP-NP-C4dAb under laser stimulation on pro-inflammatory factors in tissue were explored (Figure 5C). After MACs formation, endothelium activation induces lymphocyte migration toward the injury site for antigen clearance purpose. MCP-1 and tumor necrosis factor (TNF) initially released by the endothelium are important for macrophages and monocytes recruitment.[35] Natural killer (NK) cells are the key effector cells during microvascular graft damage in ABMR and produce IFN-γ under IL-12p70 stimulation.[36] IL-6 is a main product of inflammation, whereas IL-10 is an anti-inflammatory factor. In the allografts, increase in IL-10 level by IL-6 indicates that the local homeostasis was under stress.[37] Lower expression levels of major pro-inflammatory cytokines (IL-6, IL-10, IL-12p70, IFN-γ, TNF, and MCP-1) in both the kidney lysate and blood serums were observed in the MP and MP-NP-C4dAb + Laser treated groups of C57BL/6 mice with Allo-KT compared with those from the control group and MP-NP-C4dAb without laser treated group (Figure S8, Supporting Information). This finding indicates a reduction in endothelium activation and injury, substantial recruitment and ABMR-associated NK infiltration and a decrease in overall inflammation, as well as limited toxicity by nanoparticles after irradiation. Moreover, the transplanted renal function (albuminuria, serum creatinine (Cr) and blood urea nitrogen (BUN)) were evaluated in the urine and serum of the mice (Figure 5D). The finding showed high levels of these biomarkers which indicated that ABMR after Allo-KT caused an impairment in kidney function. On the contrary, the levels of the markers after treatment with MP and MP-NP-C4dAb with/without laser were similar to those of the Iso-KT group, indicating that kidney functions were restored after treatment of the Allo-KT group because of the reduced inflammation.

Anti-inflammatory effect of MP is attributed to modulation of gene expression and inhibition of proinflammatory cytokines. In addition, therapeutic effect of MP is associated with reduction of the number of circulating lymphocytes by inducing apoptosis of these cells. Apoptosis levels of circulating and infiltrating lymphocytes were determined to explore the systemic effect of MP on circulating lymphocytes. The effect of MP-NP-C4dAb, which has graft-targeting properties, on leukocyte apoptosis after laser irradiation was also investigated. Based on flow cytometry methods, the apoptosis rate of leukocytes in graft and peripheral blood mononuclear cell (PBMC) was evaluated by Annexin V/Propidium Iodide (PI) apoptosis assay (**Figure 6**). Annexin V is widely used together with PI to detect whether cells are viable, apoptotic, or are necrotic through determining differences in plasma membrane permeability and integrity. After intravenous injection, MP underwent blood circulation and promoted apoptosis of lymphocyte in the kidney tissue and peripheral blood (MP treated group) (Figure 6A,B). This finding indicates that MP has an effective immunosuppressive effect and can be used as a primary agent to inhibit ABMR in transplanted graft. However, it triggers significant side effects such as systemic lymphopenia. On the contrary, no significant systemic lymphopenia was observed for the MP-NP-C4dAb and MP-NP-C4dAb + Laser treated groups. Moreover, the Laser group showed a lower proportion of viable lymphocytes in the graft and a higher percentage of lymphocytes apoptosis compared with the MP group (Figure 6B). This observation indicates a higher local targeting efficacy in the graft, mainly due to the enriched local drug concentration on inflammatory sites with the C4dAb-coating. Furthermore, the drug release was precisely controlled by in-situ laser irradiation, which significantly eliminated exposure of MP to circulating lymphocytes. Moreover, therapeutic effects were centralized in the allograft site suffering from ABMR, and apoptosis was significantly up-regulated in the injured tissue. These findings imply that MP-NP-C4dAb + Laser can effectively decrease local lymphocyte infiltration in allografts with low lymphopenia in the circulation. The findings from the current study indicate that MP-NP-C4dAb + Laser exhibited excellent therapeutic effects against inflammation infiltration in Allo-KT mice and caused limited systemic side effects.

2.5. In Vivo Long-Term Toxicity Study

Treatment with MP-loaded nanoparticles enhanced immune inhibition in Allo-KT C57BL/6 mice, showing that they have great clinical potential. However, key aspects of this new generation of nanomedicine, including their bio-distribution, long-term fate, and toxicity are still poorly understood. To assess toxicity, healthy BALB/c mice (weight: 23 ± 2 g, $n = 4$) were intravenously injected with MP, MP-NP, and MP-NP-C4dAb every 3 days (as treatment groups, the dosages of drug in the MP, MP-NP, and MP-NP-C4dAb groups were equivalent to 10 mg kg^{-1} dispersed in 200 µL of PBS), followed by close monitoring for over four weeks. The control group consisted of mice injected with PBS. As shown in **Figure 7**A, within 28 days, no significant body weight change and no signs of apparent weakness or spontaneous mice death of drug-loaded nanoparticles were observed, indicating that all animal mature constantly without adverse effects. Meanwhile, serum biochemistry assay was performed to determine the potential toxicity of nanoparticles on the mice, after 28 days. A series of serum biochemical indicators were examined with particular concern

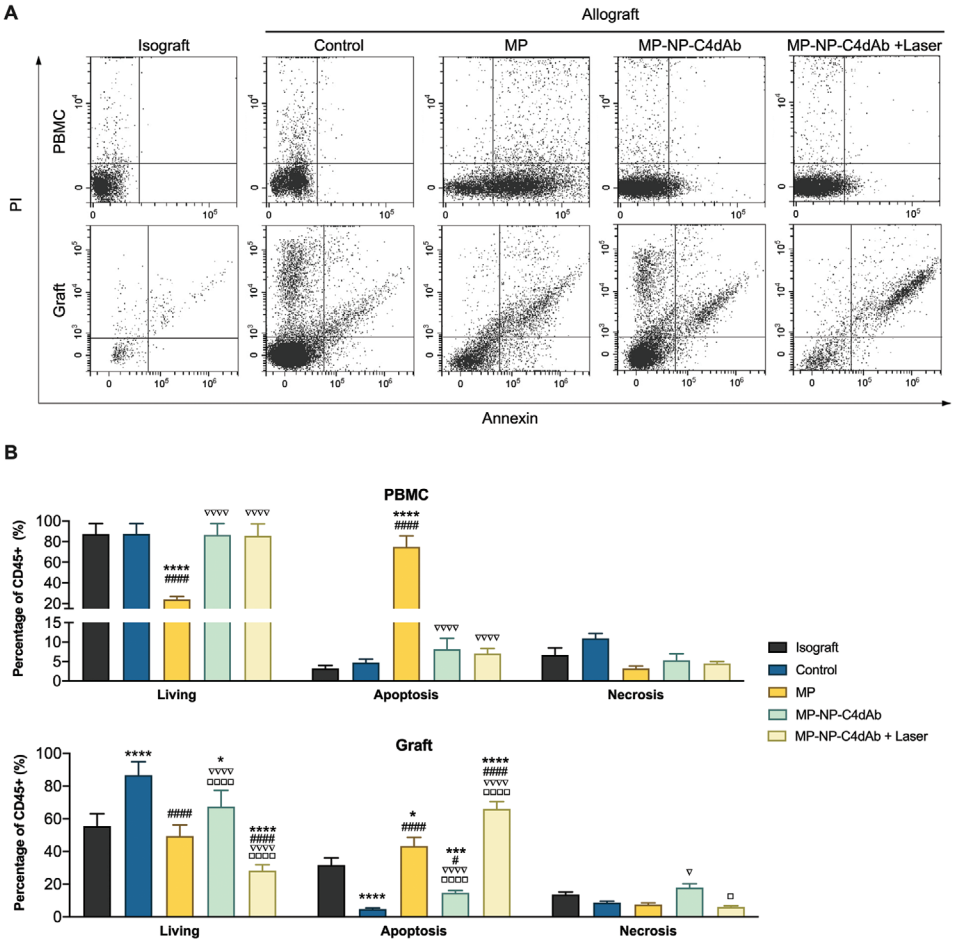

Figure 6. The apoptotic profile of leukocytes in peripheral blood mononuclear cells (PBMC) and grafts. A) Characterization of leukocyte apoptosis in graft tissue and PBMC using pure MP and MP-NP-C4dAb with/without Laser. B) Quantification of leukocyte living, apoptosis and necrosis in graft and PBMC ($n = 4$, $^{*}P < 0.05$, $^{***}P < 0.001$, $^{****}P < 0.0001$ versus Isograft. $^{\#}P < 0.05$, $^{\#\#\#\#}P < 0.0001$ versus Control. $^{\triangledown}P < 0.05$, $^{\triangledown\triangledown\triangledown\triangledown}P < 0.0001$ versus MP. $^{\square}P < 0.05$, $^{\square\square\square\square}P < 0.0001$ versus MP-NP-C4dAb, Two-way ANOVA with Tukey's multiple comparisons test).

of kidney and liver function. As shown in Figure 7B, the kidney function indicators, including Cr and BUN levels, in the treatment groups were comparable to those in the control mice. Furthermore, 28-day administration of MP increased liver function indicators such as triglyceride (TG) and total cholesterol (TC) levels in mouse liver, whereas drug-loaded nanoparticles attenuated the MP-induced liver TG and TC increase in a dose-dependent manner to levels comparable to control mice. As illustrated in Figure 7C, Oil Red O special stain is a quick and low-cost method for assessing steatosis on frozen biopsies following long-term administration. When compared to the MP injection group, the MP-NP and MP-NP-C4dAb groups showed a clear remission of hepatic steatosis. These findings reveal that NP exposure causes no evident liver or kidney damage in mice. Based on long-term biotoxicity studies, the major organs of mice were processed for H&E (**Figure 8**) and Masson (Figure S9, Supporting Information) staining and then histopathological examined to determine whether or not NP exposure caused tissue inflammation or lesions (i.e., local infiltration of inflammatory cells, shrinkage or blebbing of histocytes or interstitial deposition of collagen). After 28 days, the organs architecture from pure drug and NP treated mice exhibited little variation from the control group. In any of the treatment groups, no obvious histological abnormalities or lesions were observed. All of these findings suggested that NP injection did not cause severe toxicity.

Steroid pulse therapy for rejection was developed over a half-century ago[38] and is still widely used in clinical practice due to the significant reversal function even though it is associated with various side effects, including infections, and even death.[39] The innate immune system is the first line of defense against antigenic infection, but is impaired by high-dose steroid administration and increases the risk of infection. Thus, the most desirable immunomodulatory treatment strategy in clinical organ transplantation is to minimize immune recognition against the graft while maintaining anti-infection activity and eventually establishing graft immune tolerance. In this study, reduced lymphocyte apoptosis in peripheral circulation demonstrated that the targeted drug release decreased the systemic immune dysregulation caused by the traditional MP pulse therapy.

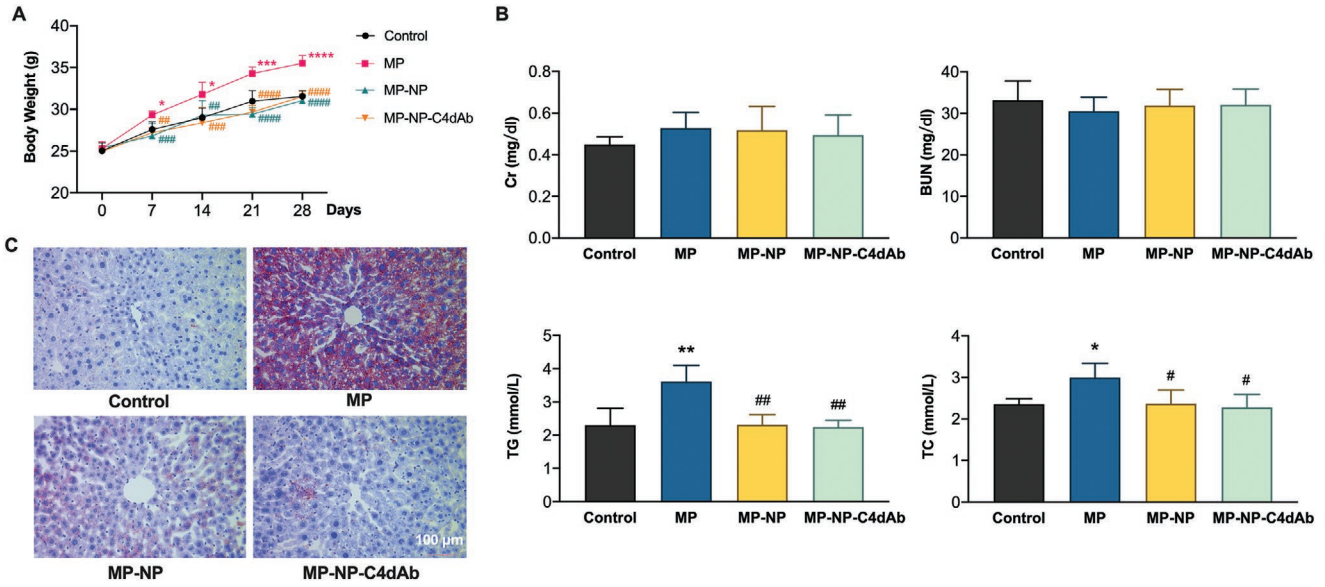

Figure 7. Long-term circulating toxicity test in vivo. A) Changes in body weight of C57BL/6 mice treated with PBS (control group), MP, MP-NP and MP-NP-C4dAb (treatment groups) at various time points. B) Serum biochemical analysis, including creatinine (Cr), blood urea nitrogen (BUN), triglyceride (TG) and total cholesterol (TC) levels in the blood were determined. C) Representative liver sections from each group of mice stained with Oil Red O ($n = 4$, $^{*}P < 0.05$, $^{**}P < 0.01$ versus Control, $^{\#}P < 0.05$, $^{\#\#}P < 0.01$, $^{\#\#\#}P < 0.001$, $^{\#\#\#\#}P < 0.0001$ versus MP, Two-way ANOVA for body weight analysis and One-way ANOVA for the serum biochemical analysis with Tukey's multiple comparisons test respectively).

This advantage is presumably due to the on-site drug release mediated by C4dAb coated nanoparticles. The clearance of MP is primarily by urine excretion, and the kidney graft localized release significantly reduced drug circulation and consumption in mice, resulting in a significant reduction in peripheral adverse effects. Another potential benefit of the transient drug release triggered by NIR is that it peaks the local drug concentration with lower dosage carried by NP in a short time, and reduces the drug amount in the future pulse steroid therapy practice, which needs to be studied further. Furthermore, pulse therapy consists of numerous high-dose injections throughout a several-day therapy period to maintain sufficient drug concentration in the lymphocyte-attacked loci. More research is needed to determine whether the programmable release of nanoparticles can transform multiple short-lasting injections into a single long-term injection using non-invasive NIR irradiation, which was not done in the recent study.

3. Conclusion

In conclusion, a novel therapeutic platform based on CuS@MSN was devised and synthesized, and surface engineered for allograft kidney endothelial antigen region targeting and in situ immune system inhibition therapy. Immunosuppressive drugs can be released controllably from nanoparticles under NIR irradiation as a promising photothermal conversion agent, and the cytocompatibility of the drug delivery system was assessed by cytotoxicity studies, which revealed that the photothermal process had a negligible effect on cellular viability and controlled drug release without exacerbating inflammation and tissue damage. We also exhibited specific and significantly increased allograft endothelium targeting of NP after conjugation with the C4d antibody in vitro and in vivo, which was further validated by non-invasive in vivo imaging, biodistribution and tissue histology studies. The targeting assay enables real-time monitoring and treatment of ABMR in all solid organ transplantation and is groundbreaking for future clinical studies based on this technology. Following the accumulation of nanoparticles in the C4d positive endothelium, irradiation of allograft with NIR, selected for greater penetration in human tissue with minimal damage, triggered the release of drugs that induce the apoptosis of inflammation recruited lymphocytes, while reducing the pro-inflammatory cytokines in the ABMR attacked graft. Notably, this process also preserved the innate immunity with a significantly limited dysfunction effect on the circulating lymphocytes, and have a significant impact on their bench-to-bedside translation. In vivo toxicity studies with nanoparticles revealed no toxicity compared with MP alone. To our knowledge, the developed MP-NP-C4dAb is one of the very few theranostic nanoparticles capable of active ABMR targeting in vivo. We will further explore the potential of these smart nanoparticles for in vivo transplanted kidney lesion targeting to prevent antigen-presenting, improve therapeutic efficacy, and reduce adverse effects.

4. Experimental Section

Materials: Copper(II) chloride ($CuCl_2$), Sodium sulfide nonahydrate ($Na_2S{\cdot}9H_2O$), Cetyltrimethylammonium chloride solution (CTAC, 25 wt%), Tetraethyl orthosilicate (TEOS), Triethanolamine (TEA), (3-Aminopropyl)triethoxysilane (APTEOS), Methylprednisolone (MP) were purchased from Sigma-Aldrich, while sulfo-Cy5.5 was purchased from Lumiprobe Corporation. Ethanol (99.5%), Sodium chloride (NaCl), were purchased from Fisher Scientific. Water and all buffers were of

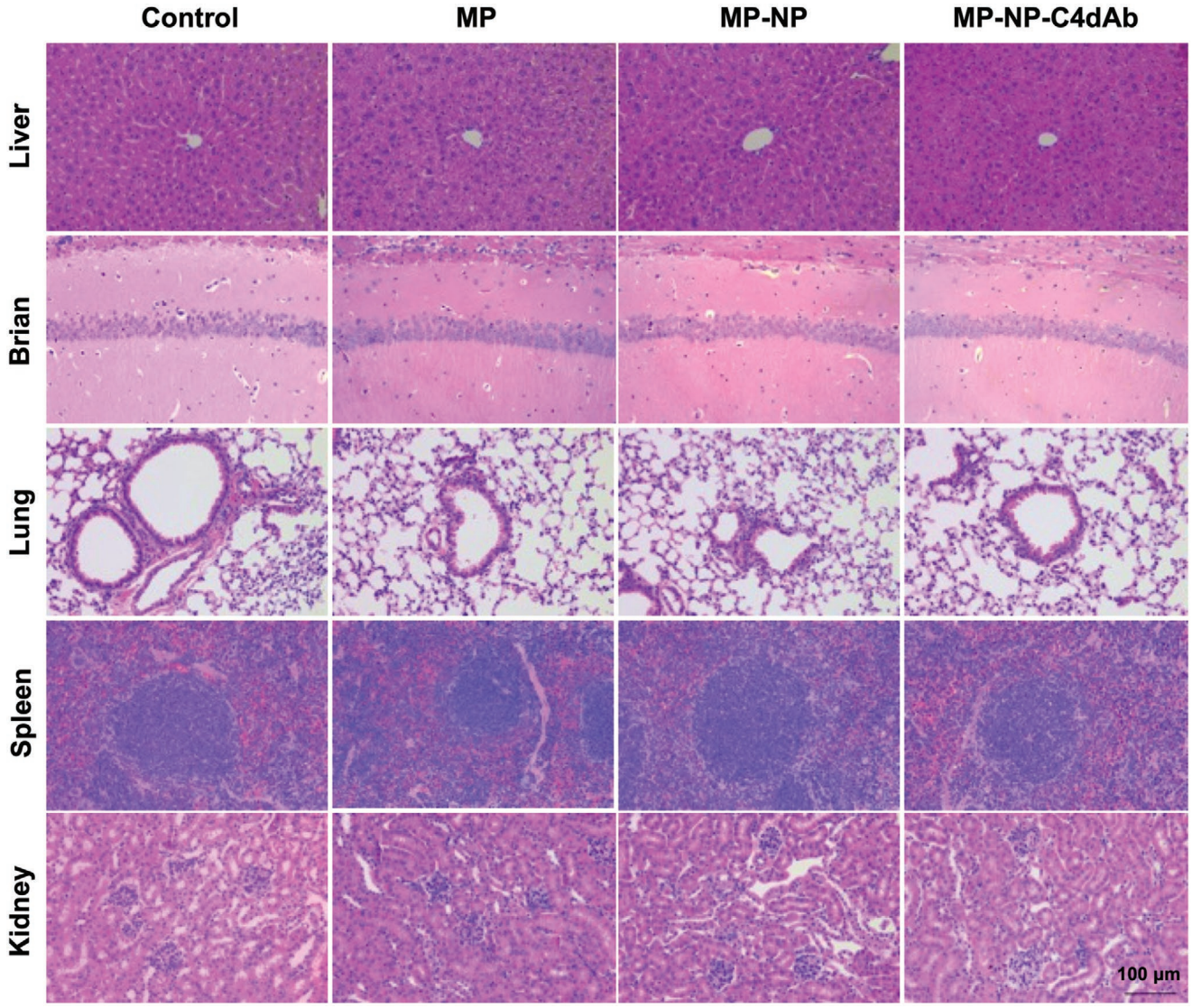

Figure 8. Histological examination to confirm long-term in vivo tissue damage distribution. After 28 days, Hematoxylin and Eosin (H&E) staining of major organs, including the liver, brain, lungs, spleen, and kidneys from mice treated with MP, MP-NP, and MP-NP-C4dAb and PBS only as control group.

Millipore grade and pretreated with Chelex 100 resin to ensure that the aqueous solution was free of heavy metals. All chemicals were used as received without further purification.

Animals: The animal experiment protocol was approved by the Research Ethics Committee of the First Affiliated Hospital, College of Medicine, Zhejiang University (No. 2019-1231) and was carried out according to the National Institutes of Health Guide for the Care and Use of Laboratory Animals (NIH Publication No. 80-23). Eight-week-old male BALB/c and C57BL/6 mice (weight: 23 ± 2 g) were purchased from the Laboratory Animal Center of Zhejiang University. The animals were unrestricted to water and standard rodent chow, and were maintained in a controlled environment (25 °C) following a 12 h light/dark cycle.

Experimental Procedures: Detailed methods are described in the Supporting Information experimental procedures.

Statistical Analysis: All statistical analyses were performed using GraphPad Prism 8 (GraphPad Inc, CA, USA). Results were displayed as mean ± standard deviation (SD) unless stated otherwise. ANOVA with Tukey's post-test was applied for multiple group comparisons. $P < 0.05$ was considered statistically significant.

Supporting Information

Supporting Information is available from the Wiley Online Library or from the author.

Acknowledgements

C.L. and P.P.Y. contributed equally to this work. This work was supported by National Natural Science Foundation of China (81770719, 81871472, and 81770750), Research Fellow (Grant No. 328933), Solution for Health Profile (336355), and InFLAMES Flagship (337531) grants from Academy of Finland, Finland China Food and Health International Pilot Project funded by the Finnish Ministry of Education and Culture (280M0052K1), and Sigrid Jusélius Foundation. Electron microscopy samples were processed and analyzed in the Electron Microscopy Laboratory, University of Turku; Confocal/Flow cytometry were performed at the Cell Imaging Core, Turku Bioscience Centre. Biocenter Finland is acknowledged for the supporting of those infrastructures.

Conflict of Interest

The authors declare no conflict of interest.

Data Availability Statement

The data that support the findings of this study are available on request from the corresponding author. The data are not publicly available due to privacy or ethical restrictions.

Keywords

antibody-mediated rejection, anti-inflammation, controlled drug release, kidney transplantation, targeting delivery

Received: November 3, 2021
Revised: January 21, 2022
Published online:

[1] V. A. Luyckx, M. Tonelli, J. W. Stanifer, *Bull World Health Organ* **2018**, *96*, 414.

[2] a) S. Davis, J. E. Cooper, *Transplant. Rev. (Orlando)* **2017**, *31*, 47; b) B. J. Nankivell, S. I. Alexander, *N. Engl. J. Med.* **2010**, *363*, 1451; c) J. Bamoulid, O. Staeck, T. Crepin, F. Halleck, P. Saas, S. Brakemeier, D. Ducloux, K. Budde, *Nephrol. Dial Transplant.* **2017**, *32*, 1601; d) J. A. Galian, A. Mrowiec, M. Muro, *Expert Opin. Ther. Targets* **2016**, *20*, 859; e) P. S. Macklin, P. J. Morris, S. R. Knight, *Transplant. Rev. (Orlando)* **2017**, *31*, 87.

[3] R. A. Wolfe, V. B. Ashby, E. L. Milford, A. O. Ojo, R. E. Ettenger, L. Y. Agodoa, P. J. Held, F. K. Port, *N. Engl. J. Med.* **1999**, *341*, 1725.

[4] a) J. M. Piper, W. A. Ray, J. R. Daugherty, M. R. Griffin, *Ann. Intern. Med.* **1991**, *114*, 735; b) A. L. Buchman, *J. Clin. Gastroenterol.* **2001**, *33*, 289.

[5] a) R. R. M. Correa, J. R. Machado, M. V. da Silva, F. R. Helmo, C. S. O. Guimaraes, L. P. Rocha, A. C. G. Faleiros, M. A. dos Reis, *Clin Dev Immunol* **2013**, *2013*, 678180; b) Z. Kikic, A. Kainz, N. Kozakowski, R. Oberbauer, H. Regele, G. Bond, G. A. Bohmig, *Clin. J. Am. Soc. Nephrol.* **2015**, *10*, 1435.

[6] a) V. Nickeleit, M. J. Mihatsch, *Nephrol. Dial Transplant.* **2003**, *18*, 2232; b) H. E. Feucht, H. Schneeberger, G. Hillebrand, K. Burkhardt, M. Weiss, G. Riethmuller, W. Land, E. Albert, *Kidney Int.* **1993**, *43*, 1333; c) A. B. Collins, E. E. Schneeberger, M. A. Pascual, S. L. Saidman, W. W. Williams, N. Tolkoff-Rubin, A. B. Cosimi, R. B. Colvin, *J. Am. Soc. Nephrol.* **1999**, *10*, 2208.

[7] a) M. C. Fishbein, J. Kobashigawa, *Curr. Opin. Cardiol.* **2004**, *19*, 166; b) K. Murata, W. M. Baldwin, 3rd, *Transplant. Rev. (Orlando)* **2009**, *23*, 139.

[8] D. C. Mastellos, D. Ricklin, E. Hajishengallis, G. Hajishengallis, J. D. Lambris, *Mol. Oral Microbiol.* **2016**, *31*, 3.

[9] M. Wang, J. A. Zuris, F. Meng, H. Rees, S. Sun, P. Deng, Y. Han, X. Gao, D. Pouli, Q. Wu, I. Georgakoudi, D. R. Liu, Q. Xu, *Proc. Natl. Acad. Sci. USA* **2016**, *113*, 2868.

[10] a) H. Auvinen, H. Zhang, Nonappa, A. K. , E. H. Niemela, S. Nummelin, A. Correia, H. A. Santos, V. Linko, M. A. Kostiainen, *Adv. Healthcare Mater.* **2017**, *6*, 1700692; b) F. Kong, H. Zhang, X. Qu, X. Zhang, D. Chen, R. Ding, E. Makila, J. Salonen, H. A. Santos, M. Hai, *Adv. Mater.* **2016**, *28*, 10195.

[11] H. Zhang, D. Liu, M. A. Shahbazi, E. Makila, B. Herranz-Blanco, J. Salonen, J. Hirvonen, H. A. Santos, *Adv. Mater.* **2014**, *26*, 4497.

[12] Z. Liu, Y. Li, W. Li, C. Xiao, D. Liu, C. Dong, M. Zhang, E. Makila, M. Kemell, J. Salonen, J. T. Hirvonen, H. Zhang, D. Zhou, X. Deng, H. A. Santos, *Adv. Mater.* **2018**, *30*, 1703393.

[13] a) M. P. Ferreira, S. Ranjan, A. M. Correia, E. M. Makila, S. M. Kinnunen, H. Zhang, M. A. Shahbazi, P. V. Almeida, J. J. Salonen, H. J. Ruskoaho, A. J. Airaksinen, J. T. Hirvonen, H. A. Santos, *Biomaterials* **2016**, *94*, 93; b) H. Zhang, W. Cui, X. Qu, H. Wu, L. Qu, X. Zhang, E. Makila, J. Salonen, Y. Zhu, Z. Yang, D. Chen, H. A. Santos, M. Hai, D. A. Weitz, *Proc. Natl. Acad. Sci. USA* **2019**, *116*, 7744.

[14] Y. Qiao, Y. Ping, H. Zhang, B. Zhou, F. Liu, Y. Yu, T. Xie, W. Li, D. Zhong, Y. Zhang, K. Yao, H. A. Santos, M. Zhou, *ACS Appl. Mater. Interfaces* **2019**, *11*, 3809.

[15] D. Liu, H. Zhang, B. Herranz-Blanco, E. Makila, V. P. Lehto, J. Salonen, J. Hirvonen, H. A. Santos, *Small* **2014**, *10*, 2029.

[16] a) C. Sahlgren, A. Meinander, H. Zhang, F. Cheng, M. Preis, C. Xu, T. A. Salminen, D. Toivola, D. Abankwa, A. Rosling, D. S. Karaman, O. M. H. Salo-Ahen, R. Osterbacka, J. E. Eriksson, S. Willfor, I. Petre, J. Peltonen, R. Leino, M. Johnson, J. Rosenholm, N. Sandler, *Adv. Healthcare Mater.* **2017**, *6*, 1700258; b) M. H. Yao, M. Ma, H. B. Zhang, Y. Z. Zhang, G. Wan, J. Shen, H. R. Chen, R. Wu, *Adv. Funct. Mater.* **2018**, *28*, 1804497; c) Y. H. Ma, F. H. Cai, Y. Y. Li, J. H. Chen, F. Han, W. Q. Lin, *Bioact. Mater.* **2020**, *5*, 732.

[17] a) Q. J. He, J. L. Shi, *Adv. Mater.* **2014**, *26*, 391; b) D. Tarn, C. E. Ashley, M. Xue, E. C. Carnes, J. I. Zink, C. J. Brinker, *Acc. Chem. Res.* **2013**, *46*, 792.

[18] a) K. Welsher, Z. Liu, S. P. Sherlock, J. T. Robinson, Z. Chen, D. Daranciang, H. J. Dai, *Nat. Nanotechnol.* **2009**, *4*, 773; b) N. Li, P. X. Zhao, D. Astruc, *Angew. Chem., Int. Ed.* **2014**, *53*, 1756.

[19] a) Q. Tian, J. Hu, Y. Zhu, R. Zou, Z. Chen, S. Yang, R. Li, Q. Su, Y. Han, X. Liu, *J. Am. Chem. Soc.* **2013**, *135*, 8571; b) T. Yang, Y. Wang, H. Ke, Q. Wang, X. Lv, H. Wu, Y. Tang, X. Yang, C. Chen, Y. Zhao, H. Chen, *Adv. Mater.* **2016**, *28*, 5923; c) M. Zhou, J. Li, S. Liang, A. K. Sood, D. Liang, C. Li, *ACS Nano* **2015**, *9*, 7085.

[20] a) L. Guo, I. Panderi, D. D. Yan, K. Szulak, Y. Li, Y. T. Chen, H. Ma, D. B. Niesen, N. Seeram, A. Ahmed, B. Yan, D. Pantazatos, W. Lu, *ACS Nano* **2013**, *7*, 8780; b) Z. Y. Xiao, *Nanomedicine* **2014**, *9*, 373.

[21] X. Zhang, P. P. Yang, Y. L. Dai, P. A. Ma, X. J. Li, Z. Y. Cheng, Z. Y. Hou, X. J. Kang, C. X. Li, J. Lin, *Adv. Funct. Mater.* **2013**, *23*, 4067.

[22] a) Z. L. Tang, Y. Akiyama, T. Okano, *J. Polym. Sci., Polym. Phys. Ed.* **2014**, *52*, 917; b) S. Y. Lu, B. Li, B. L. Ni, Z. H. Sun, M. Z. Liu, Q. Wang, *Soft Matter* **2011**, *7*, 10763.

[23] M. Zhou, R. Zhang, M. Huang, W. Lu, S. Song, M. P. Melancon, M. Tian, D. Liang, C. Li, *J. Am. Chem. Soc.* **2010**, *132*, 15351.

[24] a) Q. Tian, F. Jiang, R. Zou, Q. Liu, Z. Chen, M. Zhu, S. Yang, J. Wang, J. Wang, J. Hu, *ACS Nano* **2011**, *5*, 9761; b) Q. Tian, M. Tang, Y. Sun, R. Zou, Z. Chen, M. Zhu, S. Yang, J. Wang, J. Wang, J. Hu, *Adv. Mater.* **2011**, *23*, 3542.

[25] D. Shen, J. Yang, X. Li, L. Zhou, R. Zhang, W. Li, L. Chen, R. Wang, F. Zhang, D. Zhao, *Nano Lett.* **2014**, *14*, 923.

[26] M. Vallet-Regi, A. Ramila, R. P. del Real, J. Perez-Pariente, *Chem. Mater.* **2001**, *13*, 308.

[27] L. Pan, Q. He, J. Liu, Y. Chen, M. Ma, L. Zhang, J. Shi, *J. Am. Chem. Soc.* **2012**, *134*, 5722.

[28] Y. L. Liu, K. L. Ai, J. H. Liu, M. Deng, Y. Y. He, L. H. Lu, *Adv. Mater.* **2013**, *25*, 1353.

[29] E. Tarabukina, E. Seyednov, A. Filippov, M. Constantin, V. Harabagiu, G. Fundueanu, *Macromol. Res.* **2017**, *25*, 680.

[30] A. Djamali, D. B. Kaufman, T. M. Ellis, W. Zhong, A. Matas, M. Samaniego, *Am. J. Transplant.* **2014**, *14*, 255.

[31] a) T. Takano, A. V. Cybulsky, *Am. J. Pathol.* **2000**, *156*, 2091; b) A. V. Cybulsky, T. Takano, J. Papillon, A. Khadir, J. H. Liu, H. W. Peng, *J. Biol. Chem.* **2002**, *277*, 41342.

[32] D. Cohen, R. B. Colvin, M. R. Daha, C. B. Drachenberg, M. Haas, V. Nickeleit, J. E. Salmon, B. Sis, M. H. Zhao, J. A. Bruijn, I. M. Bajema, *Kidney Int.* **2012**, *81*, 628.
[33] a) J. S. Chua, H. J. Baelde, M. Zandbergen, S. Wilhelmus, L. A. van Es, J. W. de Fijter, J. A. Bruijn, I. M. Bajema, D. Cohen, *J. Am. Chem. Soc.* **2015**, *26*, 2239; b) A. Vongwiwatana, S. Gourishankar, P. M. Campbell, K. Solez, P. F. Halloran, *Am. J. Transplant.* **2004**, *4*, 124; c) J. M. Gloor, F. G. Cosio, D. J. Rea, H. M. Wadei, J. L. Winters, S. B. Moore, S. R. DeGoey, D. J. Lager, J. P. Grande, M. D. Stegall, *Am. J. Transplant.* **2006**, *6*, 1841.
[34] G. H. Tse, E. E. Hesketh, M. Clay, G. Borthwick, J. Hughes, L. P. Marson, *Jove-J. Visualized Exp.* **2014**, *92*, 52163.
[35] a) T. L. Cranford, R. T. Enos, K. T. Velazquez, J. L. McClellan, J. M. Davis, U. P. Singh, M. Nagarkatti, P. S. Nagarkatti, C. M. Robinson, E. A. Murphy, *Int. J. Obesity* **2016**, *40*, 844; b) Y. Takada, T. Hisamatsu, N. Kamada, M. T. Kitazume, H. Honda, Y. Oshima, R. Saito, T. Takayama, T. Kobayashi, H. Chinen, Y. Mikami, T. Kanai, S. Okamoto, T. Hibi, *J. Immunol.* **2010**, *184*, 2671; c) W. M. Chu, *Cancer Lett.* **2013**, *328*, 222.
[36] a) E. D. Tait Wojno, C. A. Hunter, J. S. Stumhofer, *Immunity* **2019**, *50*, 851; b) M. A. O'Neill, L. G. Hidalgo, *Int. J. Immunogenet.* **2021**, *48*, 110.
[37] A. Steensberg, C. P. Fischer, C. Keller, K. Moller, B. K. Pedersen, *Am. J. Physiol. Endocrinol. Metab.* **2003**, *285*, E433.
[38] N. J. Feduska, J. G. Turcotte, J. A. Penner, G. E. Bacon, P. W. Gikas, *J. Surg. Res.* **1972**, *12*, 208.
[39] A. Sinha, A. Bagga, *Indian J. Pediatr.* **2008**, *75*, 1057.